



# INVESTIGATING THE DEPENDENCE OF FORBUSH DECREASE ON GEOMAGNETIC CUTOFF RIGIDITY

O. C. Nwuzor, O. Okike, A. E. Umahi, C. C. Nwaevo, C. I. Nworie,  
A. Ojobeagu, A. Chikwendu, C. Ozibo and P. B. Otah

(Received 8 January 2024; Revision Accepted 26 January 2024)

## ABSTRACT

The dependence of Forbush decreases on geomagnetic cutoff rigidity has been studied. The study aimed to investigate the implications of geomagnetic cutoff rigidity on forbush decrease. To achieve this aim, the data of cosmic ray daily count from six neutron stations of Tibet, Esei, Tsumeb, Oulu, Apatity, and Magadan were used. These data covered a period of six (6) years from the year 2010 to 2015. An advanced manual method developed by Okike and Umahi (2019b) was used to select the FDs through R. statistical software. A sharp depression in the intensity of cosmic ray variation known as Forbush decrease (FD) was detected. A large number of FDs were recorded. The results of our analysis was grouped into stations of high, low and middle rigidity. The stations of low rigidity recorded the highest number of FDs followed by stations of middle rigidity while the stations of high rigidity recorded the least number of FDs. The magnitude of these FDs was determined. It was observed that FD magnitudes vary inversely with the station's rigidity. A correlation between the FD magnitudes of the cosmic ray (CR) stations was also tested. It was observed that stations of low rigidity indicated the best correlation followed by the stations of middle rigidity, while the stations of high rigidity indicated the least correlation. A regression was further tested between the FD magnitudes of the different stations. The result of the regression between FDs of different stations was 99.8% , 98% and 97.5% significant for stations low, high and middle rigidity stations respectively. In summary, this study used a large number of events to test the rigidity dependence of FDs, and it was observed that FDs are inversely related to the cutoff rigidity. Thus, FDs measured at the CR stations can be used to examine the effects of rigidity between the stations.

**KEYWORDS;** Cosmic rays, Forbush decrease and geomagnetic cutoff rigidity.

## INTRODUCTION

The pioneering observation of cosmic ray (CR) variations revealed an abrupt change in CR flux intensity. This short-term intensity variation is attributed to solar wind disturbances and is generally referred to as Forbush decrease (FD) (Lee et. al., 2015). During an FD, the intensity of CR decreases rapidly (Lee et. al., 2015).

The cause of such a rapid decrease in the intensity of CR is the strong magnetic boundary against CR particles (Hundhausen 1972, Lockwood et. al., 1991) generated by interplanetary coronal mass ejections (ICMEs) (Cane, 2000) and interplanetary shock (IP shock) near the Earth. Similarly, FDs can also occur when magnetic clouds pass close to the Earth (Klein and Burlaga 1982; Zhang and Burlaga 1988, Oh et al., 2008).

**O. C. Nwuzor**, Department of Industrial Physics, David Umahi Federal University of Health Sciences, Uburu, Nigeria

**O. Okike**, Department of Industrial Physics, Ebonyi State University, Abakaliki, Nigeria.

**A. E. Umahi**, Department of Industrial Physics, Ebonyi State University, Abakaliki, Nigeria.

**C. C. Nwaevo**, Department of Industrial Physics, David Umahi Federal University of Health Sciences, Uburu, Nigeria

**C. I. Nworie**, Department of Industrial Physics, David Umahi Federal University of Health Sciences, Uburu, Nigeria

**A Ojobeagu**, Department of Industrial Physics, David Umahi Federal University of Health Sciences, Uburu, Nigeria

**A Chikwendu**, Department of Industrial Physics, David Umahi Federal University of Health Sciences, Uburu, Nigeria

**C. Ozibo**, Department of Industrial Physics, Ebonyi State University, Abakaliki, Nigeria.

**P. B. Otah**, Department of Industrial Physics, David Umahi Federal University of Health Sciences, Uburu, Nigeria

In addition, FDs are also caused by magnetic-field variations linked to the interplanetary shock-sheath region (Parker, 1961; Hundhausen, 1972; Lockwood et al., 1991) and the magnetic cloud (Klein and Burlaga, 1982; Zhang and Burlaga, 1988; Badruddin, 2002; Oh et al., 2008). In most cases, FDs have well-defined profiles with four distinct parts (e.g., Oh et al., 2008): onset, main phase, maximum depression point, and recovery phase. FDs start from the main phase of decreasing CR intensity to a recovery phase in which the CR intensity recovers resulting in a distinct FD time profile (Lee et al., 2013). The entire FD profile can take anywhere from a few hours to several days to complete (Oh et al., 2008).

The ability of CR particles to penetrate magnetic fields and reach the top of the Earth's atmosphere is controlled by rigidity ( $R$ ) which is defined as the particle's momentum multiplied by the speed of light per unit charge (Kalugin and Kabin, 2015). The geomagnetic cutoff rigidity is a notion that defines how the earth's magnetic field protects against the entrance of charged cosmic ray particles from outside the magnetosphere (Shea and Smart, 2006). It is usually measured in gigavolts (GV) (Kalugin and Kabin, 2015). Rigidities are often thought to be static (Shea and Smart, 2006). This is a common misunderstanding since the cutoff rigidity values fluctuate as the dipole and non-dipole components of the magnetic field change (Shea and Smart, 2006). The magnitude of CRs impacting the atmosphere at a certain point as a function of time is affected by these changes in geomagnetic cutoff rigidity (Shea and Smart, 2006). However, processes on the Sun can accelerate protons to relativistic energies, producing Solar Proton Events (SPE), also known as Solar Energetic Particle (SEP) events. SPE particles cannot, however, access the entire global atmosphere as they are partially guided by the geomagnetic field. The first description of cosmic rays in the Earth's magnetic field (Störmer, 1930) demonstrated the geomagnetic cutoff rigidity, the minimum rigidity a particle must possess to penetrate to a given geomagnetic latitude, where the rigidity of a particle is defined as the momentum per unit charge. Therefore, every geomagnetic position has a corresponding cutoff rigidity. Higher rigidities are required to reach lower geomagnetic latitudes, and thus all particles with rigidities larger than the minimum can penetrate to that latitude (and all higher latitudes). In general the geomagnetic cutoff rigidity of a particle is also a function of its direction of arrival. While this effect was initially modeled with a static dipole field, the geomagnetic cutoff rigidity is a much more dynamic quantity depending on the Earth's internal and external magnetic fields. As such the geomagnetic cutoff varies spatially and with time, on timescales of both the internal (years) (Smart and Shea, 2003b) and the external field (minutes/hours) (Kress et al., 2004).

The intensity at which CRs collide with the Earth's atmosphere is known as CR intensity flux (Balco, 2011). This CR intensity flux varies with latitude because it is modulated by the Earth's magnetic field (Cockburn and Summerfield, 2004). They are observed and recorded by ground-based NMs, ion chambers, balloon flights, and cosmic ray telescopes mounted on spacecraft, and satellites (Lockwood and Webber, 1977). Based on the advantages of the rigidity and coordinates of the ground-based neutron monitors, data from these monitors are always preferably used and reviewed in CR research. In the early analyses of FDs, the rigidity dependence of the amplitude of the decrease at high rigidities was obtained primarily from neutron monitor data (Lockwood, 1991).

Previous research on FDs has identified two methods of FD selection that are commonly used by researchers. These methods of FD selections are (i) the manual method and (ii) the automated method. The manual method of FD selection involves several stages: (1) Defining a certain threshold or baseline ( $B$ ) reduction in CR flux intensity, (2) Normalizing CR intensity data using a chosen running mean, (3) Trial and error method, involving plotting CR data for some equal intervals of time, calculating the percentage change (concerning the running mean) of the normalized CR data at the onset time ( $I$ ) and the percentage change at the time of maximal ( $I$ ) depression,  $\min(I)$  (4) Subtracting  $I$  from  $I$  and deciding whether  $I - \min(I) \geq B$ ,  $\max(I)$  (5) Deciding the events for which  $I - \min(I) \geq B$  (that  $\min(I)$  will qualify for FDs) and the rest discarded as non-FD event and, (6) Estimating either the onset time or time of maximal decreases of all the events that meet the condition in (5) (see Okike, 2019; Harrison & Ambaum, 2010; Kristjansson et al., 2008; Oh, Yi, & Kim, 2008, for details of the approach). A close inspection of Fig. 1 by Harrison and Ambaum (2010) suggests that each of the steps is subject to several potential biases.

The automated method differs significantly from the manual technique. The automated method uses a program that views CR data as a Fourier series and thus, transforms CR data using the Fourier Transform Technique (FTT). The manual approach involves the tedious and time-consuming task of culling and plotting CR data for a few selected days, judging whether the plotted data reflect a typical FD profile, examining the various parts of the plotted FD such as onset time, main phase, and time of maximal depression, calculating the level of intensity increases or reductions and so on, the automated method handles the CR data as a single signal, irrespective of the volume. After the Fourier transformation and filtering of the unwanted signals, a script for FD event identification is written in an R language for statistical computing (Team, 2014). The algorithm takes the Fourier-transformed signal as its input data. It scans the data, picking all the pits/peaks/depressions/troughs. Another subroutine

identifies the time of the depressions/peaks and passes the results to some subprograms that perform several other tasks such as determining the static mean of the input data, isolating pits from peaks, estimating the amplitude of the depressions concerning the calculated average, and so on.

However, the FDs obtained from these methods are subject to validation. For instance, Kristjansson et al. (2008), identified 22 large FDs between 2000 and 2005 using Climax data. They validated the dates of these events by comparing them with FDs found in another two stations, the Oulu and Moscow stations. An event is said to be an FD if the CR data are equal to or lower than a certain baseline for instance 5% below the 90-day running mean.

Research has revealed a dependence of geomagnetic cutoff rigidity and coordinates on FDs. Belov et al., (2021) suggested that low energies (rigidities) seem to be better suited for studying the fine structure of interplanetary disturbances (primarily interplanetary coronal mass ejections) that lead to FDs. Webber (1962) estimated that after the three large decreases occurring in July 1959, the total integral intensity of CR particles with rigidities greater than about 1 GV at the Earth decreased to only 20% of the intensity at sunspot minimum when the CR intensity is at its maximum. According to Tanabashi et al. (2018), CRs are a population of high-energy elementary particles and nuclei of strong penetrating power that originate in outer space and within our galaxy. Jamsen et al., (2007) used three events to study the energy dependence on the recovery time of FDs and opined that the recovery time of an FD can strongly depend on the energy. Lingri et. al., (2016) equally used three events to study the dependence of FDs on rigidity and found that each NM records FDs.

Over the past decades, a phenomenological understanding of galactic cosmic ray (GCR) intensity modulation has remained a hot research area in astrophysics. While some authors attribute the variations in the count rate of NM stations which in turn influences Fds to altitude and rigidity, others are of the view that other factors may also aid such variations. However, previous research such as (Ahluwalia and Fikani, 2007; Lockwood et. al., 1991) used a few events to test the rigidity dependence of Fds and concluded that Forbush decreases amplitudes vary inversely with rigidity. Although insufficient data was available to these authors, this limited their conclusions. However, the reliability of the results obtained using these few events to test the rigidity dependents of FDs is highly questionable. Thus, to generate more reliable results, a larger number of events are needed to test the rigidity dependents of FDs. Therefore, this work aims at using a large number of events to test the rigidity dependence of FDs. This will provide a broader view of the rigidity dependence of FDs because several events will be considered, and the bias of whether

FDs are strongly or weakly dependent on rigidity will be cleared.

## MATERIALS

The major materials that were used for this research are the daily CR data that was obtained from <http://cr0.izmiran.ru/common/> for six CR stations. The six CR stations and their corresponding cutoff rigidity are TIBT (14.10GV), ESOI (10.8GV), OULU (0.77GV), MGDN (2.11GV), APTY (5.6GV) and TSMD (9.21GV). These data covered the period of six years between the years 2010 to 2015. The data of solar wind speed (SWS) and interplanetary magnetic field (IMF) were also used and sourced from <https://omniweb.gsfc.nasa.gov/html/owdata.html> for the same period under study. R. Statistical software and a laptop computer were equally used for the statistical analysis

## METHODS

The methods applied in this research are grouped under the following subsections;

### Data harvesting

The daily data of cosmic rays were sourced from the Izmiran website for all thirteen cosmic ray stations and the period under study. These daily data were placed and arranged in a text editor software. The 00 hours as contained in the raw data were filtered off from the CR data since we are working with daily counts. The data after arrangement contains only the dates and the CR counts in a well-arranged tabular form. They were further saved with a unique file name for each neutron station. In addition, the solar wind speed (SWS) and interplanetary magnetic field data were also sourced from the internet and arranged in a tabular form. The data covers the same period as that of CR. They were filtered to the tune of dates and counts on the process of the download using the website data query. They were also further saved with unique file names.

### Data Processing

The advanced manual method of FD selection was used in this work. These method involves the use of computer software program that is operated using R. statistical software. The method of program FD event location developed by Okike and Umahi (2019) was employed in the present investigation. In brief, the technique employs Fourier transformation techniques in an attempt to filter several signals of different periodicities that are naturally superimposed on CR data. Some of these amplitude variations are very similar to FDs and could have serious influence on the FD magnitude as well as frequency estimations if they are not carefully removed before searching for FDs. One of such unwanted signals is CR diurnal anisotropies. Low and high pass filters implemented in the Fast Fourier algorithm are used to separate long-term trend and daily variations from the high frequency part of CR data. The high frequency signal consists of high magnitude CR events such as ground level enhancement (GLE), solar energetic

particles (SEPs) and FDs. A pit and peak detector program is written in a software called R for statistical computing (Team,2014). Using some predefined baselines, the magnitudes / amplitudes and event

$$\hat{g}(k) = \int d^n x g(x) e^{-ixk}$$

The corresponding inverse Fourier transform is

$$\hat{g}(x) = \int \frac{d^n k}{(2\pi)^n} \hat{g}(k) e^{ik.x}$$

It is, however, more useful to consider the discrete Fourier transform for computational purposes. In particular, we used the FFT algorithm implemented in the R language for statistical computing.

When z is an array storing the values to be transformed, the fft usage is `fft(z, inverse = FALSE)`.

$$x[h] = \sum_{k=1}^n z[k] \times \exp(-2 \times \pi \times 1i \times (k - 1) \times \frac{h-1}{n})$$

for  $h = 1, \dots, n$ , and  $n = \text{length}(x)$ . If `inverse` is `TRUE`,  $\exp(-2 \times \pi \dots)$  is replaced with  $\exp(2\pi \dots)$ . When z contains an array, `fft` computes and returns the multivariate (spatial) transform. If `inverse` is `TRUE`, the (non-normalized) inverse Fourier

$$CR(\%) = \frac{CR - CR_q}{CR_q} \times 100\%$$

where  $CR_q$  represents the mean value of the CR data for the period of interest. After normalization and filtering of the low- and high-frequency signals by Fourier transformation, the R code searches for the minimum turning points and calculates their amplitudes (FDs) as well as their time of occurrence in the high-frequency data.

In Summary, the processes and stages involved in this method are as explained below;

$$CR(\%) = \frac{CR - CR_q}{CR_q} \times 100\%$$

(d) It further plotted the normalized CR counts with dates. This indicated decreases in the variations of CR counts by giving a baseline for FD detection using an abline along the CR variations.

(e) A threshold of  $< -0.5\%$  was used as a baseline for FD mgnitude selection

(e) The program then filtered the observed variation for the first time using a red plotted points.

(f) It further filtered the variations for the second time by feeding the program with the identified FD dates and magnitudes to indicate a clearer point of FDs in the third plot.

time of the big as well as the small pits / depressions are estimated. These amplitudes and the corresponding dates are taken as FD data. Readers are referred to Okike and Umahi (2019) for more details on the operations of the two algorithms. Wherein, For an n-dimensional function  $g(x)$ , the Fourier transform can be defined as;

$$(1)$$

$$(2)$$

For `inverse = TRUE`, the `fft` function would compute the non-normalized inverse transform.

If the array z is vectorized, then the value returned after FFT computation is the non-normalized univariate discrete Fourier transform containing the sequence of values in the array z. That is, `x <-z` returns

$$(3)$$

transform is returned, i.e., if `x <-fft(z)`, then z is `fft(x, inverse = TRUE)/length(x)`. The normalization method adopted by Tezari et al. (2016) using Equation 4 is also implemented in the Fourier algorithm,

$$(4)$$

(a) The program restructured the raw CR data into a unique nature of dates and counts. It further saves same with a unique fine name.

(b) The program read the file as saved in (a) above, scale and plot the daily variations of the CR counts for the period under study.

(c) The program normalized the daily CR counts using

$$(4)$$

The list of FD dates and magnitudes was presented. The FD dates were presented separately in a tabular form followed by that of the magnitude which was presented as an FD catalogue. These lists of FDs were grouped into three phases according to the cut-off rigidity of their respective neutron stations. The phases include FDs of stations of high, low, and middle rigidity. They were further presented in a tabular form following this order of the three phases. The corresponding SWS and IMF data were equally placed side by side with the FDs and presented in a tabular form. The presentation was equally done in three phases according to the CR station's cut-off rigidity of high, low, and middle rigidity.

A correlation test between some selected FD magnitudes and the station's geomagnetic cutoff rigidity was done. The FD used for this correlation is the event of 26-05-2013 was used to test the simultaneity of FDs of high rigidity while the events of 02-03-2015 and 24-06-2011 for low and middle rigidity stations. These events were similar in date to the classifications of the stations under study. The correlation plot was presented while the station's geomagnetic cut-off rigidity and FD magnitudes were also presented in a tabular form. Also performed is the correlation test

between FD magnitudes of stations against stations. This test was grouped into stations of high, low, and middle cut-off rigidity. The correlation table containing the correlation coefficients was presented. The correlation plots were also presented.

A multiple regression was thereafter tested between (a) FDs of stations and (b) FDs with SWS and IMF. The essence of the regression is to further validate our results on the relationships tested.

**RESULTS**

Figs 1a & b shows the variation of raw cosmic ray data while Figs 2a&b show the filtration of the cosmic ray data to indicate better points of FDs.

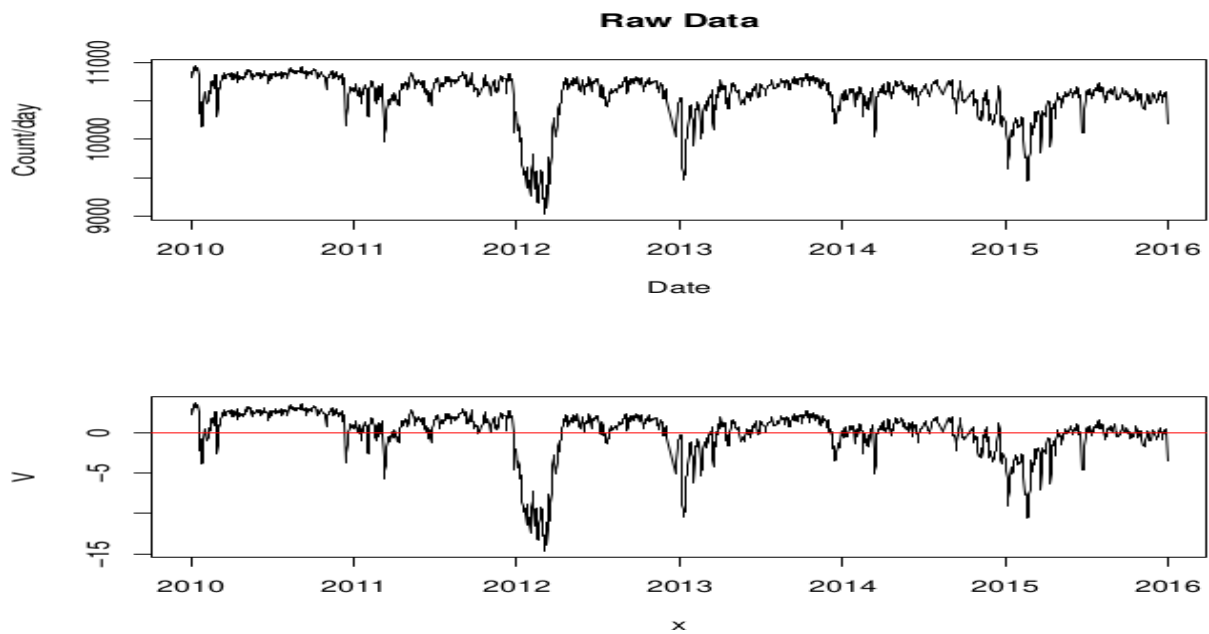


**Fig 1: (a) Variations of cosmic ray raw data. (b) Variations of cosmic ray raw data showing a baseline for FD selection**

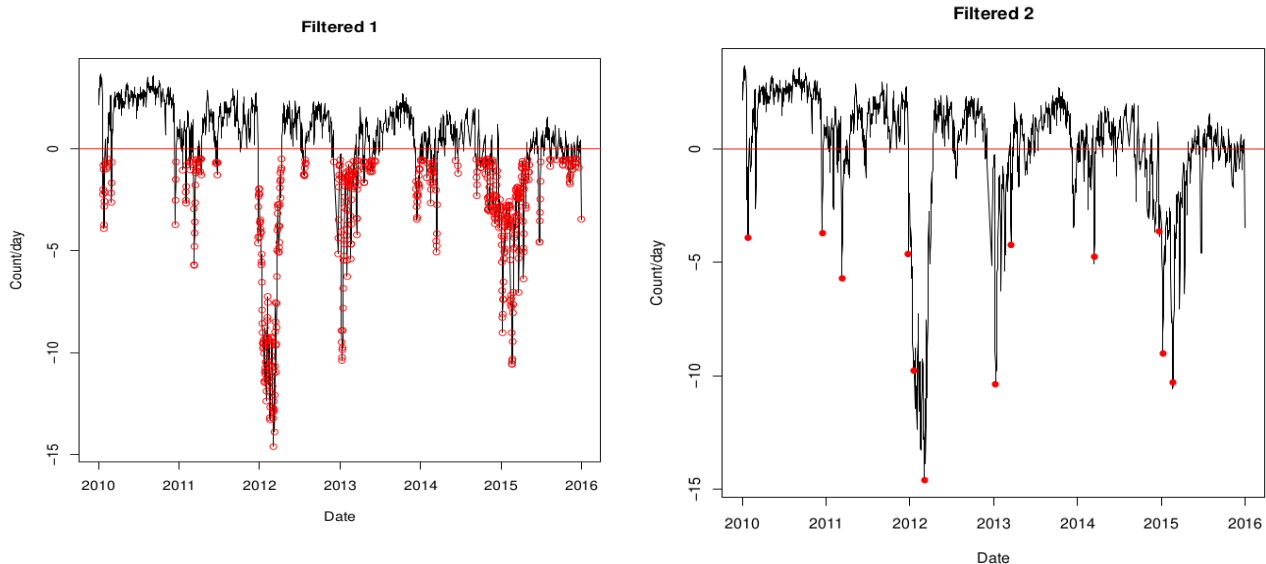


**Fig. 2 a & b: First and second filtration of FDs**

The selected FD dates and magnitudes from six CR stations of TIBT, ESOI, OULU, MGDN, APTY, and TSMD are grouped into three stations of high, low, and middle cut-off rigidity and sampled in Table 1 – 3 below. Table 1 which stands for stations of high cut-off rigidity contains the detected FD dates and magnitudes of the two CR stations of ESOI and TIBT, while Tables 2 and 3 which stand for stations of low

and middle rigidity contain two CR stations of OULU and MGDN, and two CR stations of APTY and TSMD respectively. These FD dates and magnitudes were generated from our filtration of CR data and our method of FD detection. The tables contain the samples of the FD dates and magnitudes as the generated FDs are so large. A total of 484 FDs were observed in the TIBT neutron station while 548 events were observed in ESOI neutron stations as shown in Table 1 and appendices for stations of high rigidity.

**Table 1: Determined FD magnitudes for stations of high cut-off rigidity**

TIBT		ESOI	
Date	FD (%)	Date	FD (%)
2011-04-07	-0.53	2010-01-21	-2.24
2011-04-08	-1.03	2010-01-22	-2.01
2011-04-09	-0.55	2010-01-23	-0.82
2011-06-14	-0.54	2010-01-24	-1.03
2011-06-17	-1.5	2010-01-25	-3.93
2011-06-18	-1.61	2010-01-26	-3.75
2011-06-19	-1.48	2010-01-27	-2.83
2011-06-20	-1.03	2010-01-28	-2.58
2011-06-21	-0.77	2010-01-29	-2.15
2011-06-22	-0.8	2010-01-30	-0.74

**Table 2: Determined FD magnitudes for stations of low cut-off rigidity.**

OULU		MGDN	
DATE	FD (%)	Date	FD (%)
2010-07-27	-8.92	2011-04-08	-0.98
2011-04-08	-0.51	2011-06-11	-0.61
2011-06-17	-1.56	2011-06-17	-1.53
2011-06-18	-1.73	2011-06-18	-1.61
2011-06-19	-1.18	2011-06-19	-1.31
2011-06-20	-0.54	2011-06-20	-0.69
2011-06-23	-2.17	2011-06-23	-1.73
2011-06-24	-3.57	2011-06-24	-3.64
2011-06-25	-3.03	2011-06-25	-3.12
2011-06-26	-2.03	2011-06-26	-2.12

**Table 3: Determined FD magnitudes for stations of middle cut-off rigidity**

APTY		TSMD	
Date	FD (%)	Date	FD (%)
2011-04-07	-0.57	2011-03-30	-0.74
2011-04-08	-0.73	2011-04-03	-0.71
2011-06-11	-0.53	2011-04-04	-0.52
2011-06-17	-1.82	2011-04-06	-0.83
2011-06-18	-1.88	2011-04-07	-1.16
2011-06-19	-1.19	2011-04-08	-1.94
2011-06-20	-0.62	2011-04-09	-1.12
2011-06-23	-2.3	2011-04-10	-0.74
2011-06-24	-3.84	2011-04-11	-0.65
2011-06-25	-3.24	2011-04-12	-0.72

The Pearson correlation approach was used to test for correlations between FDs of the CR stations used

in this work, based on our classifications of CR stations of high, low, and middle cutoff rigidity. The general Pearson correlation formula is;

$$r = \frac{\sum_{j=1}^k (x_j - \bar{x})(y_j - \bar{y})}{\sqrt{\sum_{j=1}^k (x_j - \bar{x})^2 \sum_{j=1}^k (y_j - \bar{y})^2}} \tag{2}$$

(Okwonu et al., 2020)

Where  $r$  = correlation coefficient,  $\bar{x} = \frac{\sum_{j=1}^k x_j}{k}$  and  $\bar{y} = \frac{\sum_{j=1}^k y_j}{k}$  are the sample means. Note that  $(x_j, y_j, j = 1, \dots, n)$  are data points from two variables assumed to be normally distributed with parameters  $\mu^x, \mu^y, \delta_{\mu^x}^2, \delta_{\mu^y}^2$ .

The correlations are grouped into three phases. Phase one shows the correlation between the FD magnitudes of the stations while phase two shows the correlation between the FD magnitudes and their corresponding solar wind and interplanetary magnetic field data. The results of these correlations are shown with tables and plots.

**Table 4: Correlation results of FDs from stations of high rigidity**

S/no	Stations	Correlation coefficient
1	TIBT vs ESOI	0.23

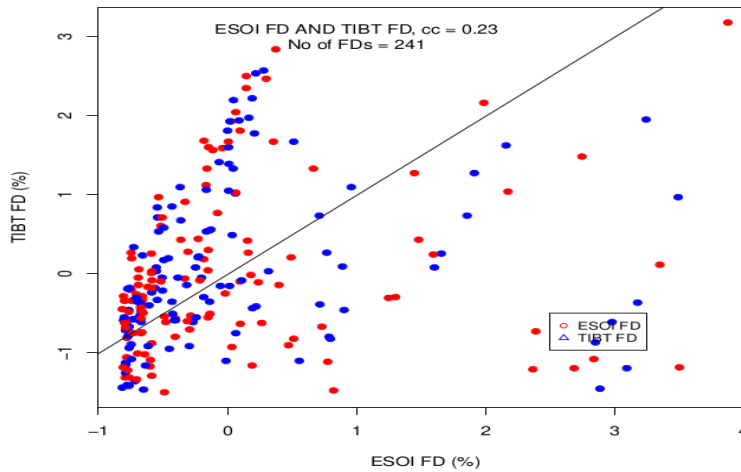


**Fig. 3: Correlation plot of ESOI and TIBT**

**Table 5: Correlation results of Fds from stations of low cut-off rigidity**

S/no	Stations	Correlation coefficient
1	TERA vs SOPO	0.97

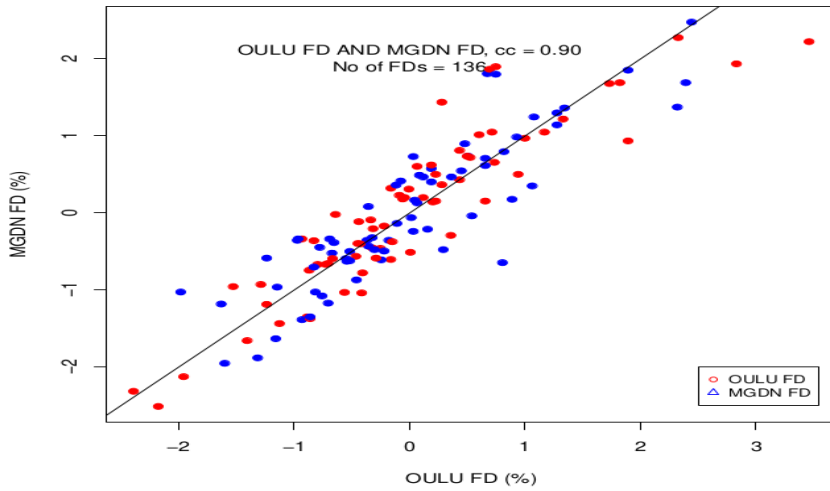


Fig. 4: Correlation plot of MGDN and OULU FDs

Table 6: Correlation results of Fds from stations of low cut-off rigidity

S/no	Stations	Correlation coefficient
1	TSMD vs APTY	0.82

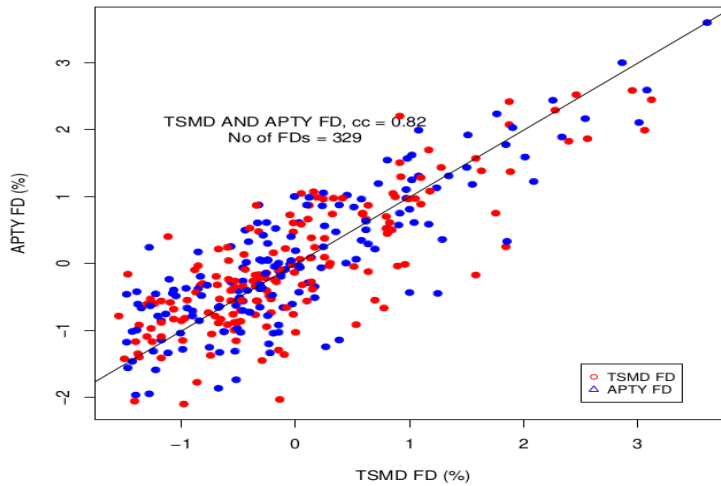


Fig. 5: Correlation plot of TSMD and APTY FDs

The results of the regression test are grouped into three phases. Phase one shows the regression between the FD magnitudes of the stations while phase two shows the regression between the FD magnitudes and their corresponding solar wind and interplanetary magnetic field data. Multiple regression method was used for the regression test. The results of these regressions are shown with plots below.

The regression between FD magnitudes of CR stations is grouped into three. The first group represents the stations of high rigidity while the second and the third represent the stations of low

and middle cut-off rigidity respectively. Generally, the regression equations are of the form;

$$y = c + mx \tag{2a}$$

Where c = intercept, m = slope

Fig. 6 shows the regression plot between FDs of ESOI and TIBT stations which represents the station as of high cut-off rigidity. The regression equation is given as;

$$FD_{ESOI} = 1.58 \pm 0.08 + (0.07 \pm 0.02) FD_{TIBT} \tag{3}$$

Note that  $R^2 = 0.83$ , the p-values of intercept (I) and slope (S) are  $<2 \times 10^{-16}$  and 0.00030, respectively, and N (i.e. the number of simultaneous FDs) is 241.

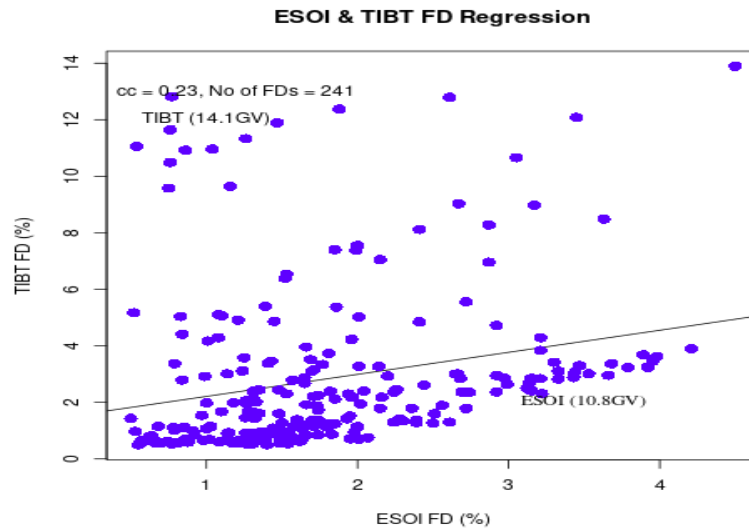


Fig. 6: Regression of FDs of ESOI and TIBT stations

Fig. 7 shows the regression plot between FDs of OULU and MGDN stations which represents the station as of low cut-off rigidity. Their corresponding regression equations and details are as given as equations 4 as shown below:

$$FD_{OULU} = 0.78 \pm 0.19 + (1.0 \pm 0.04) FD_{MGDN} \quad (4)$$

$R^2 = 0.80$ , the p-values of intercept (I) and slope (S) are  $7.69 \times 10^{-5}$  and  $<2 \times 10^{-16}$ , respectively, and N (i.e. the number of simultaneous FDs) is 136.

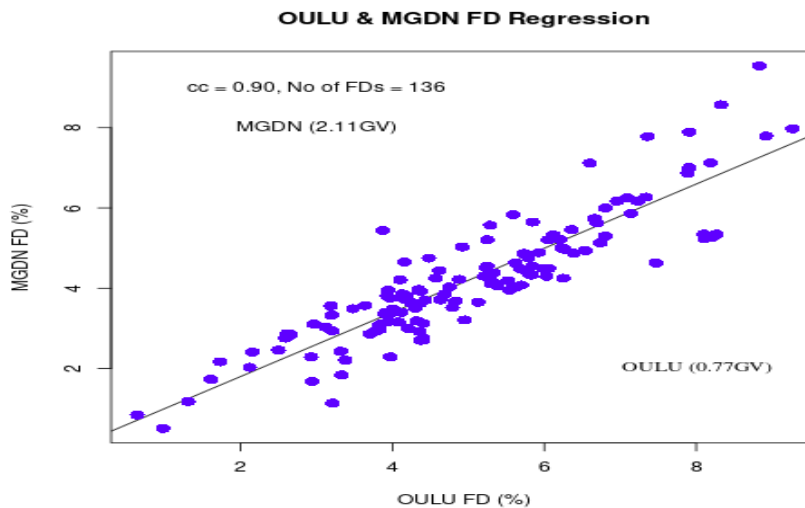
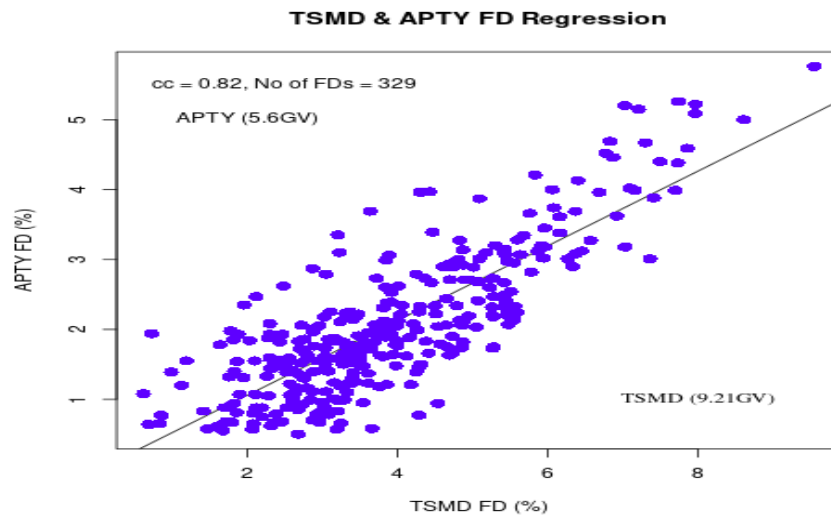


Fig. 7: Regression of FDs of OULU and MGDN stations

Fig. 8 shows the regression plot between FDs of TSMD and APTY stations which represents the station as of middle cut-off rigidity. Their corresponding regression equations and details are as given as equations 5 as shown below:

$$FD_{TSMD} = 1.29 \pm 0.11 + (1.26 \pm 0.05) FD_{APTY} \quad (5)$$

$R^2 = 0.68$ , the p-values of intercept (I) and slope (S) are  $<2 \times 10^{-16}$  and  $<2 \times 10^{-16}$ , respectively, and N (i.e. the number of simultaneous FDs) is 327.



**Fig. 8: Regression of FDs of TSM D and APTY stations**

### DISCUSSION

Table 1, 2, and 3 above shows our selected FD dates and magnitudes. The selected FDs were categorized into three based on the cutoff rigidity of the CR stations under study. The categories include stations of high, low, and middle rigidity. The FD dates and magnitudes of the stations of high rigidity were presented in Table 1 while those of low and middle rigidity were presented in Tables 2 and 3 respectively. From Table 1, it was observed that the TIBT station recorded 484 FDs while the ESOI station recorded 548 FDs. These two stations were used to represent the stations of high rigidity. From Table 2 it was observed that a total of 1101 and 1104 FDs were recorded for OULU and MGDN neutron stations respectively. These two stations were used to represent the stations of low rigidity. From Table 3, it was observed that a total of 1004 and 745 FDs were observed for APTY and TSM D neutron stations respectively. These two stations were used to represent the stations of middle cut-off rigidity.

A close study and comparison of the selected FDs as sampled in Tables 1, 2, and 3 indicated some variations. While the CR stations with low cut-off rigidity consistently recorded the highest number of FDs followed by that of middle cut-off rigidity, the stations with high cut-off rigidity recorded the least number of FDs. For instance, while the OULU station which is of low rigidity recorded 1101 FDs, TIBT which is of high cut-off rigidity recorded 484 FDs. This finding is in agreement with Belov et al., (2021), which suggested that the amplitude of the FDs was found to decrease as the rigidity increased. The APTY station which falls within the range of stations of middle rigidity recorded 1004 FDs which is near to that of low rigidity. However, because altitude and rigidity determine the sensitivity of NMs, the trade-off between the stronger rigidity of TIBT and the smaller rigidity of OULU is expected to result in similar detection efficiency. This is in agreement with the result obtained. Some event dates were observed to

be similar to those of similar rigidity stations. These similar dates validate our result since research has proven that stations of similar rigidity mostly produce simultaneous FDs.

The magnitude of an FD is the strength/size of the depression in cosmic ray intensity variation. Tables 1, 2, and 3 show the determined FD magnitudes for neutron stations of high, low, and middle, cut-off rigidity respectively. Previous research has shown that the magnitude of FDs depends on the rigidity of neutron monitors. For instance, Belov et. al., (2021), suggested that as a general trend, the amplitude of the FDs was found to decrease as the rigidity increased. It was observed that the OULU station of low rigidity recorded a large magnitude of FDs. For instance, the highest FD was recorded on 28-06-2013 with a magnitude of -14.44% for the OULU station which has a low rigidity of 0.77GV. The same was also found on the FDs of the MGDN station. Generally, the stations with low rigidity produce a greater number of FD magnitudes. However, the small events do not show a very deep depression. These small FDs are sometimes seen to be the non-simultaneous (Oh et. al., 2008; Okike and Collier, 2011a) FD types that are not usually observed by all the stations. Tezari and Mavromichalaki (2016) suggested that these small events are affected by diurnal anisotropy, unlike the large ones. Contrarily, the stations with high rigidity had low FD magnitudes. For instance, the lowest FDs were detected on 09-10-2010 and 09-12-2015 which had a magnitude of 0.5% for TIBT and ESOI respectively which have a high rigidity of 14.10GV and 10.80GV respectively. However, the stations with high rigidity produce a lesser number of FD magnitudes. For instance, the TIBT station recorded a total of TIBT station recorded 484 FDs while the ESOI station recorded 548 FDs. This also confirms the assertion of Belov et. al., (2021) that the amplitude of the FDs was found to decrease as the rigidity increased. Generally, large Forbush events tend to show a clear deep

depression. In addition to these two cases of stations of low and high rigidity, the FD magnitudes of stations of middle rigidity were found to be both slightly high and low in value. For instance, while the station of APTY with a moderate rigidity of 5.6GV recorded a magnitude of 11.32% for the FD of 09-03-2012, the station of TSMD with a moderate rigidity of 9.21GV recorded a magnitude of 0.52% for the FD of 14-07-2012.

Research has suggested that FD magnitudes correlate with the rigidity of neutron stations. For instance, Lockwood, (1971) opined that neutron station rigidity is positively correlated with FD magnitudes, which implies that the lower the cutoff rigidity, the greater the variation in the recorded CR intensity. A strong correlation was found to exist between the FD magnitudes of the stations. Tables 6, 7, and 8 show the correlation coefficients of the FDs of these stations according to high, low, and middle rigidity stations. A correlation coefficient of  $cc = 0.23$  was found for TIBT, and ESOI which represent the stations of high rigidity, while a correlation coefficient of  $cc = 0.90$  was found for stations of OULU and MGDN which represents the stations of low rigidity. Also, a correlation coefficient of  $cc = 0.82$  was found for stations of TSMD and APTY which represents the stations of middle rigidity. The strong and positive correlations found between FDs of stations of low cutoff rigidity indicates similarity between the FDs which implies that the detection of the FDs by the neutron monitors are dependent on the cutoff rigidity which determines the sensitivity of the neutron monitors. On the other side, the weak correlation found between the FDs of the high cutoff rigidity indicates a weak relationship between the FDs which implies that other factors than cutoff rigidity may affect the sensitivity of the neutron monitors. A comparison of these correlations shows that the stations of low rigidity indicated the best correlation followed by the stations of middle rigidity, while the stations of high rigidity indicated the least correlation. These findings are in agreement with the suggestion that the magnitude of FDs is dependent on rigidity. Also, our results are in agreement with the suggestion of Okike and Nwuzor (2020) that the FDs measured at the stations can be used to examine the effects of rigidity between the two stations. However, Todd and Kniveton (2001) stated that they analyzed FDs at three high-latitude stations (NWRK, MCMC, and SOPO). Although they did not indicate the outcome of their comparison nor the implication of the result obtained, the general underlying assumption among researchers conducting FD-based correlation/regression or epoch investigation is that FDs that are simultaneous at two or more stations are strong events. Between the years 2000 and 2005, Kristjansson et al., (2008) selected 22 FDs using CLMX data and following the same approach, they simply stated that their FD event days were compared with those at Oulu and Moscow NMs, and by extension, they assumed that

their FDs are consistent, or rather simultaneous. Fig 3 shows the correlation plot of ESOI and TIBT FDs which stands for stations of high rigidity. A total of 241 events which were simultaneous for the two stations were used for this plot. The cluster of the plotted points along the fitted line indicates a good correlation between the FDs of the two stations. Fig. 4 shows the correlation plots of stations of low rigidity. Fig. 4 shows the correlation plot of OULU & MGDN stations. A total of 139 FDs which were simultaneous for the two stations were used for the correlation plot. The good cluster of the plotted points along the fitted line indicates a strong correlation between the FDs of these stations. Similarly, Fig. 5 shows the correlation plots of stations of middle rigidity. The figure shows the correlation results of TSMD and APTY stations. A total of 329 FDs which were simultaneous for all these stations were used for the correlation plot. The better cluster of the plotted points along the fitted line indicates a better correlation between the FDs of these stations.

From the results of our analysis, it was observed that the FDs measured at the stations can be used to examine the effects of geomagnetic cutoff rigidity between two stations. The results of our regression analysis were majorly categorized into two, the regression between FDs of different stations and the regression between FDs with SWS and IMF.

The regression between FDs of different stations was further sub-classified into stations of high, low, and middle cutoff rigidity. The simultaneous FDs for these stations were used for the regression test. From the results of the test, the best regression was found among stations of low cutoff rigidity.

On the other side, a weaker regression was found between FDs of high and middle rigidity stations. For instance, a weak regression was found between the FDs of ESOI and TIBT stations which represent the stations of high cutoff rigidity.

In addition, the regression between FDs of TSMD and APTY which represent the stations of middle rigidity was also found to be weak when compared to that of low rigidity stations.

This regression is significant at 97.5 %. This indicated a similar relationship between the FDs of the two stations.

Because altitude and rigidity determine the sensitivity of NMs, the trade-off between the low rigidity of TERA and SOPO is expected to result in similar detection efficiency. This is in agreement with the result obtained.

However, there are several other factors, other than rigidity or real effects from FDs that could influence the variations in the count rate of NM stations. Atmospheric depth, pressure, temperature, relative humidity, local wind speed, the rotation of the Earth concerning the acceptance cone of the detectors, latitudinal effects, instrumental variations, a station's sensitivity to CR modulation, equatorial anisotropy, North-South anisotropy, geomagnetic variations, snow, limited cone of acceptance, spurious

modulation, magnetospheric effects or imperfections in the present results are some of the agents that might be responsible for the larger FD magnitudes measured at stations of low cutoff rigidity (see Barrantes et al. 2018; Belov et al. 2018, for example).

## CONCLUSION

This work concludes that FDs are inversely related to the geomagnetic cutoff rigidity. Thus, FDs measured at the CR stations can be used to examine the effects of rigidity between the stations.

## REFERENCES

- Anastasia T., Helen M., Dimitrios K., Anastasios K., Sofia K., Christina P., and Maria A., 2016. Latitudinal and longitudinal dependence of the cosmic ray diurnal anisotropy during 2001–2014, *Ann. Geophys.*, 34, 1053–1068.
- Ahluwalia H. S., Fikani M. M., 2007. Cosmic ray detector response to transient solar modulation: Forbush decreases. *Journal of Geophysical Research*, 112(A8).
- Badruddin B., 2002. Transient modulation of cosmic ray intensity: Role of magnetic clouds and turbulent interaction regions, *Astrophys. Space Sci.*, 281, 651–661.
- Balco, G., 2011. Contributions and unrealized potential contributions of cosmogenic-nuclide exposure dating to glacier chronology, 1990-2010. *Quaternary Science Reviews*, 30(1-2):3-27.
- Barrantes M., Valdés-Galicia J. F., Musalem O., Hurtado A., Anzorena M., García R., Taylor R., Muraki Y., Matsubara Y., Sako T., Sasai Y., Hinaro N., Tateiwa N., Tsujihara H., González L. Ortiz X., E., Shibata S., Watanabe K., Sakai T., 2018. Atmospheric corrections of the cosmic ray fluxes detected by the Solar Neutron Telescope at the Summit of the Sierra Negra Volcano in Mexico. *Geofís. Intl*, 57(4).
- Belov, A., Papaioannou, A., Abunina, M., Dumbovic, M., Richardson, I.G., Heber, B., Kuhl, P., Herbst, K., Anastasiadis, A., Vourlidis, A. and Eroshenko, E., 2021. On the Rigidity Spectrum of Cosmic-Ray Variations within Propagating Interplanetary Disturbances: Neutron Monitor and SOHO/EPHIN Observations at ~ 1–10 GV. *The Astrophysical Journal*, 908(1):5.
- Cane H.V., 2000. Coronal mass ejections and Forbush decreases, *SSRv* 93, 55–77. <http://dx.doi.org/10.1023/mA:1026532125747>.
- Cockburn, H.A.P. and Summerfield M.A., 2004. Geomorphological applications of cosmogenic isotope analysis. *Progress in Physical Geography*, 28(1):1-42.
- Harrison R. G., Ambaum Maarten H.P., 2010. Observing Forbush decreases in cloud at Shetland. *Journal of Atmospheric and Solar-Terrestrial Physics*, 72(18).
- Hundhausen A. J., 1972. *Coronal Expansion and Solar Wind*. Springer, New York.
- Kalugin G. and Kabin K., 2015. An analysis of large Forbush decrease events using phase diagrams of view channels of the Nagoya multidirectional muon telescope, *Journal of Atmospheric and Solar-Terrestrial Physics*, 123, 124-136.
- Klein L. W. and Burlaga L. F., 1982. Interplanetary magnetic clouds At 1 AU. *Journal of Geophysical Research*, 87(A120):613-624.
- Kress B. T., M. K. Hudson, K. L. Perry, and P. L. Slocum 2004. Dynamic modeling of geomagnetic cutoff for the 23–24 November 2001 solar energetic particle event, *Geophys. Res. Lett.*, 31, L04808, doi:10.1029/2003GL018599.
- Kristjansson, J. E., Stjern, C.W., Stordal, F., Fjaraa, A.M., Myrhre, G., and Jonasson, K., 2008. Cosmic rays, cloud condensation nuclei and clouds – a reassessment using MODIS data. *Atmos. Chem. Phys. Discuss.* 8, 13265. DOI.
- Lee S.S., Oh S.Y. and Yi Y., 2013. Simultaneity of Forbush decrease events observed at middle-latitude neutron monitor Ahlers and Mertsch, 2015. Small-Scale Anisotropies of Cosmic Rays from Relative Diffusion. *Phys. Rev. Lett*, arXiv: 1506.05488 [astro-ph.HE]s, *JGR* 118, 608-614. <http://dx.doi.org/10.1002/jgra.50159>.
- Lee S., Oh S., Yu Y., Paul E., Geonhwa J., and Hwajin C., 2015). Long-term Statistical Analysis of the Simultaneity of Forbush Decrease Events at Middle Latitudes. *J. Astron. Space Sci.*, 32(1):33-38

- Lockwood J. A., Webber W.R. and Debrunner H., 1991. Forbush decreases interplanetary magnetic field disturbances: Association with magnetic clouds, *JGR* 96, 11587–11604.  
<http://dx.doi.org/10.1029/91JA01012>.
- Lockwood, J.A. and Webber W.R., 1967. Differential response and specific yield functions of cosmic-ray neutron monitors. *J. Geophys. Res.*, 72, 3395.
- Lockwood, J. A., Webber, W. R. and Debrunner, H., 1991. The rigidity dependence of forbush decreases observed at the earth. *J. Geophys. Res.*, 96, 5447.
- Oh S.Y., Yi Y. and Kim Y.H., 2008. Globally nonsimultaneous Forbush decrease events and their implications, *JGR* 113, A01103.  
<http://dx.doi.org/10.1029/2007JA012333>
- Okike, O. and Collier, A.B., 2011a. A multivariate study of Forbush decrease simultaneity. *J. Atmos. Solar-Terr. Phys.* 73, 796.
- Okike O. and Nwuzor O. C., 2020. Investigation of the rigidity and sensitivity dependence of neutron monitors for cosmic ray modulation using algorithm-selected Forbush decreases. *MNRAS* 493, 1948–1959.
- Okike O., 2019. Chree Method of Analysis: A Critique of Its Application to Forbush Events Selection Criteria and Timing. *The Astrophysical Journal*, 882:15.
- Okike, O. and Umahi, A.E. 2019b. The Emperical Implication of Conducting a Chree Analysis Using Data from Isolated Neutron Monitors. *Solar Physics*, 294 (2). doi: <https://doi.org/10.1007/s11207-019-1405-y>
- Parker E. N., 1961. The sudden expansion of the corona following a large solar flare and the attendant magnetic field and cosmic ray effects. *ApJ*, 133, 1014–1033.  
<http://dx.doi.org/10.1086/147105>
- R. Development Core Team R, 2014. *A Language and Environment for Statistical Computing*. R Foundation for Statistical Computing. Vienna, Austria. R Foundation for Statistical Computing, Vienna.
- Shea M.A. and Smart D.F., 2006. Geomagnetic cutoff rigidities and geomagnetic coordinates appropriate for the Carrington flare Epoch. *Advances in Space Research*, 38:209–214.
- Smart, D. F., and M. A. Shea 2003b. Geomagnetic cutoff rigidity calculations at 50-year intervals between 1600 and 2000. *Proc. ICRC 2003*, 4201-4204, Universal.
- Störmer, C. 1930. Periodische Elektronenbahnen im Feld eines Elementarmagnetron und ihre Anwendung auf Bruches Modellversuche und auf Eschenhagens Elementarwellen des Erdmagnetismus. *Zeitschr. f. Astrophys.*, 1, 237-274.
- Tanabashi M. et al., 2018. Cosmic rays. *Phys. Rev., D* 98, 030001
- Todd, M.C and Kniveton, D.R., 2001. Changes in cloud cover associated with Forbush Decreases galactic cosmic rays. *Journal of Geophysical Research-Atmospheres*, 106 (D23) 32031 – 32042.  
[10.1029/2001JD000405](https://doi.org/10.1029/2001JD000405).
- Zhang, G., and Burlaga L. F., 1988. Magnetic clouds, geomagnetic disturbances, and cosmic ray decreases. *J. Geophys. Res.*, 93, 2511–2518.